Superlattices and Microstructures, Vol. 32, Nos 2–3, 2002
doi:10.1016/S0749-6036(02)00120-9

AFM local oxidation nanopatterning of a high mobility shallow 2D hole gas

L. P. ROKHINSON[†‡], D. C. TSUI
Department of Electrical Engineering, Princeton University, Princeton, NJ 08544, U.S.A.
L. N. PFEIFFER, K. W. WEST
Bell Laboratories, Lucent Technologies, Murray Hill, NJ 07974, U.S.A.

(Received 22 August 2002)

The recently developed AFM local anodic oxidation (LAO) technique offers a convenient way of patterning nanodevices, but imposes even more stringent requirements on the underlying quantum well structure. We developed a new very shallow quantum well design which allows the depth and density of the 2D gas to be independently controlled during the growth. A high mobility (0.5×10^6 cm^2 V^{-1} s^{-1} at 4.2 K) 2D hole gas just 350 Å below the surface is demonstrated. A quantum point contact, fabricated by AFM LAO nanopatterning from this wafer, shows nine quantum steps at 50 mK.

Key words: GaAs/AlGaAs shallow hole gas, quantum point contact, AFM lithography.

The rapidly developing area of physics of nanodevices laid down new demands on heterostructure design, for example, a shallow 2D gas is required in order to improve size control and enhance the confining potential. Even more stringent requirements are imposed by recently developed AFM local anodic oxidation nanolithography (LAO), which promises a low-energy high resolution alternative to conventional e-beam lithography [1–3]. A key to the success of LAO is the properly designed heterostructure. The maximum depth of the LAO grown oxide is 100–150 Å, and shifting the surface by this amount should effectively deplete the underlying 2D gas. Experimentally it has been deduced that the 2D gas should be $<$400 Å below the surface [4]. In conventionally grown shallow modulation doped quantum wells (QWs) δ-doping provides carriers to the 2D gas and compensates the surface potential of GaAs. There is a delicate balance between underdoping, when most of the carriers are trapped at the surface and no carriers left to form the 2D gas, and overdoping, when the δ-doping layer becomes conducting at low temperatures. An addition of another doping layer at the other side of the QW reduces the necessary amount of the dopants in the top layer, but precise control of the final density of the 2D gas is still difficult.

We developed a novel heterostructure design that does not suffer from either of the above-mentioned drawbacks. The as-grown structure of a shallow p-type QW consists of a GaAs buffer grown on a [$\bar{3}$11] substrate, followed by 3000 Å AlGaAs ($x = 0.32$), Si δ-doping (6×10^{11} cm^{-2}), 500 Å AlGaAs setback, 150 Å GaAs QW, 100 Å AlGaAs barrier, 100 Å GaAs, Si δ-doping (5×10^{12} cm^{-2}), and 150 Å

[†]Author to whom correspondence should be addressed. E-mail: leonid@ee.princeton.edu.

[‡]Present address: Department of Physics, Purdue University, W. Lafayette, IN 47907, U.S.A.

0749–6036/02/080099 + 04 $30.00/0

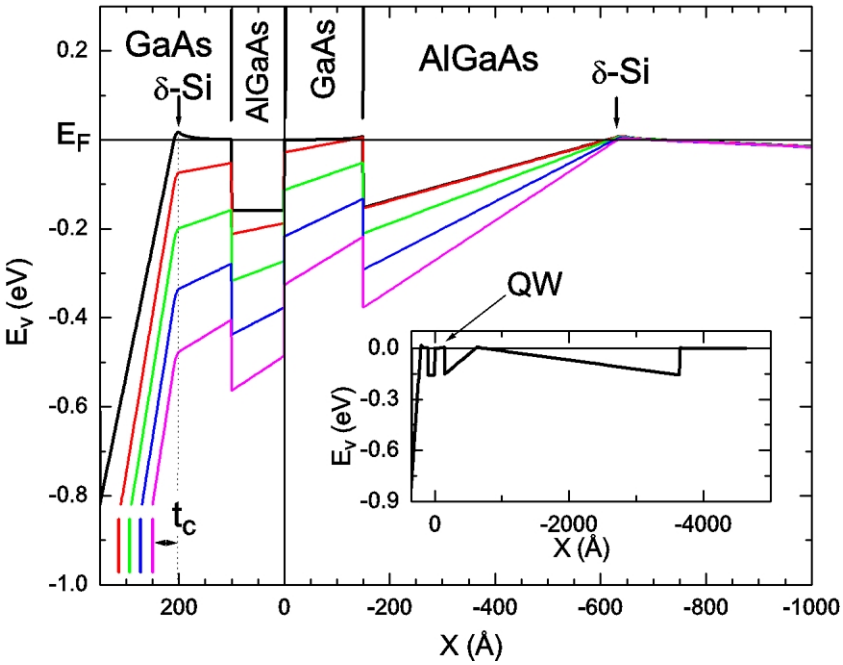

Fig. 1. Calculated band diagram for the heterostructure discussed in the text. Different curves correspond to the different thicknesses of the cap layer $t_c = 50$, 70, 90, 110 and 150 Å; vertical lines indicate position of the surface. The band diagram for the full depth of the MBE growth, calculated for $t_c = 150$ Å, is shown in the inset.

GaAs cap layer. The calculated band diagram of this structure is plotted in Fig. 1 [5–7]. The top δ-doping resides in GaAs and serves the purpose of compensating the surface potential and pinning the valence band edge E_V at the Fermi energy E_F. The doping should be low enough to avoid conduction through this layer at low temperatures. The design relaxes the criticality of the exact amount of doping because this doping layer does not provide carriers to the underlying 2D gas. The carriers are supplied by the bottom δ-doping. Again, the design provides some window for the doping concentration because the density of the 2D gas is determined by the setback thickness. An excessive doping leads to the outdiffusion of dopants toward the QW and degradation of the mobility [8]. Indeed, we have grown two wafers with the concentration of the bottom doping different by a factor of three; both QWs have hole concentrations differing by $<5\%$, but the wafer with lower doping has eight times higher mobility.

The band diagram is very sensitive to the thickness of the GaAs cap layer t_c and, thus, is ideal for LAO nanolithography. In Fig. 1 we simulated the effect of the LAO by reducing the t_c by the oxide thickness. The 2D hole gas is depleted when $t_c \sim 110$ Å, which corresponds to the oxide thickness of 60 Å. 100 Å of the oxide is estimated to lower the E_V in the QW region by 200 meV below the E_F, creating the corresponding barrier for the adjacent 2D hole gas.

We have grown a wafer using the above parameters. The wafer has the hole density 1.38×10^{11} cm^{-2} and mobility 0.48×10^6 cm^{-2} V^{-1} s^{-1} at 0.3 K, the highest reported for so shallow (350 Å below the surface) a 2D hole gas. An AFM image of a quantum point contact, fabricated from this wafer using AFM LAO, is shown in the inset in Fig. 2. The profile of the oxide is plotted in the top inset. The position of the first energy level E_0 in the QW, relative to the level position far from the oxide line, is extracted from the band calculations and plotted with black dots. Due to the nonmonotonic dependence of the E_0 on the oxide thickness, the width of the potential barrier is narrower, by factor of 2, than the thickness of the oxide line and

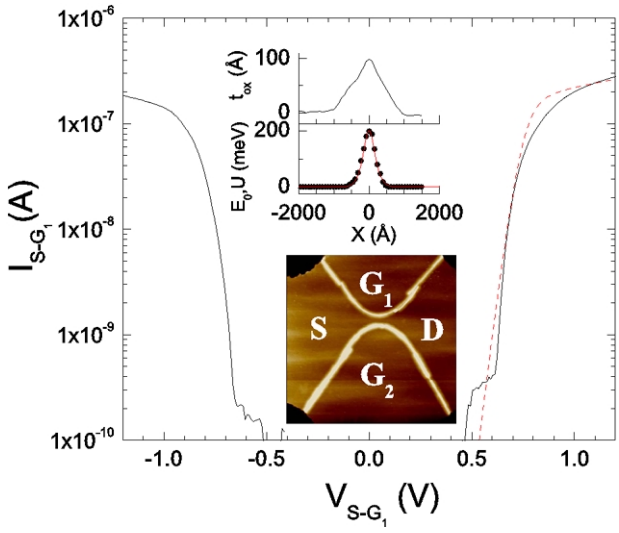

Fig. 2. Current–voltage (IV) characteristic across the oxide line (solid line). Dashed line is the calculated IV using the model potential discussed in the text. In the top inset AFM measured oxide profile t_{ox} and the corresponding calculated lowest energy in the QW E_0 (dots), see Fig. 1, are plotted. Solid line is the model potential $U(x)$ with $U_0 = 200$ meV, $V = 0$ and $\alpha = 45$ Å^{-1}. The bottom inset is a 2 μm $\times$ 2 μm AFM micrograph of the point contact, white lines are the oxide lines, black corners are the edges of the mesa.

is ≈440 Å at half height. The current–voltage (IV) characteristic across the oxide line, measured at 4.2 K, is shown in Fig. 2. The current is negligible at $|V| < 0.6$ V and there is a sharp turn on of the current at ≈0.6 V. We model the IV characteristic by calculating the tunneling probability through the barrier

$$U(x) = \frac{U_0}{\cosh^2(\alpha x)} + \frac{V/2}{\tanh(\alpha x)},$$

where U_0 is the height of the potential under the center of the oxide line, V is the applied voltage, and α^{-1} is related to the width of the oxide line. This potential [9] provides a good approximation to the expected potential, see the solid line in the inset in Fig. 2. The turn on voltage is not very sensitive to α at low temperatures for our barrier widths, as well as to the exact shape of the potential. The calculated current is plotted in Fig. 2 with the dashed line. The turn on voltage for $U_0 = 200$ meV is close to the experimentally measure one. This value of U_0 is consistent with the estimate of the tunneling barrier for 100 Å oxidation from band calculations. Experimentally, the IV characteristic is linear for oxidation depths <60 Å, indicating that no tunneling barrier is formed, also consistent with the band calculations.

Finally, we present transport characteristics of the point contact. In Fig. 3 differential conductance G is plotted as a function of the gate voltage $V_g = V_{g1} = V_{g2}$ at 50 mK. The G is quantized in units of $2e^2/h$, and up to nine plateaus can be clearly seen. A large number of steps indicate low disorder in the vicinity of the point contact. Thus, the designed heterostructure, in combination with LAO technique, provides an easy and reliable method of fabricating high quality nanostructures with sub-nanometer control over the size, shape and position.

Previously, it has been shown that the position of the change can be shifted by applying a voltage difference between the gates [10]. Moreover, the barrier width under the oxide and, correspondingly, the electrostatic coupling, can also be adjusted. The effect is the best demonstrated at elevated temperatures, when steps are smeared out and the dG/dV_g slope reflects the electrostatic coupling between the gates and the 1D channel. In the inset in Fig. 3 G is plotted as a function of $V_{g1} = V_{g2} + \Delta V_g$ for different values of ΔV_g at 4 K. The slope dG/dV_g increases with the increase of $|\Delta V_g|$, indicating large electrostatic coupling between one

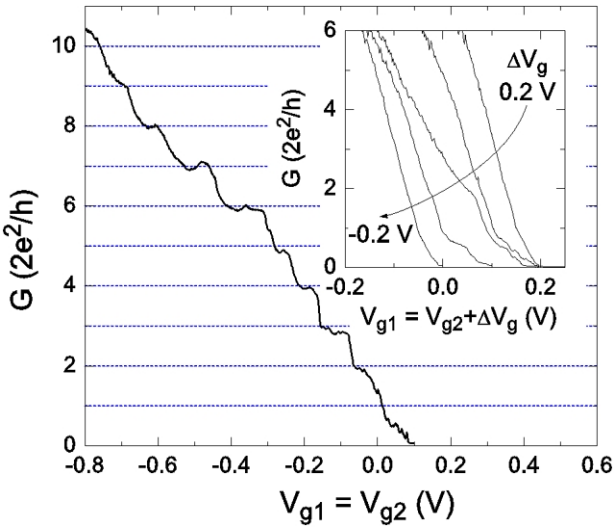

Fig. 3. Conductance G as a function of the gate voltage $V_g = V_{g1} = V_{g2}$ is measured at 50 mK. In the inset G is measured at 4.2 K while a constant voltage difference $\Delta V_g = -0.2, -0.1, 0, 0.1$ and 0.2, is applied between the gates.

of the gates and the channel. This enhancement is due to nonliner dependence of both channel and barrier widths on the gate voltage for in-plane gates [11].

To summarize, we developed a novel heterostructure design for reliable and reproducible growth of high mobility shallow QWs. We demonstrate the design by fabricating a high quality quantum point contact from such a wafer using the AFM local anodic oxidation technique. We show that the amplitude of potential barriers, formed by local oxidation of the surface, can be reliably predicted using readily available numerical simulation tools.

Acknowledgements—We thank EV Tsiper for discussions. The work was supported by a DURINT grant through the ONR and MARCO Focused Research Center on Materials, Structures, and Devices which is funded at the MIT, in part by MARCO under contract 2001-MT-887 and DARPA under grant MDA972-01-1-0035.

References

[1] E. S. Snow and P. M. Campbell, Appl. Phys. Lett. **64**, 1932 (1994); E. S. Snow and P. M. Campbell, Science **270**, 1639 (1995).
[2] X.-Z. Bo *et al*., Mater. Res. Soc. Symp. Proc. **686**, A6.5.1 (2002).
[3] R. Held *et al*., Appl. Phys. Lett. **71**, 2689 (1997).
[4] R. Held *et al*., Appl. Phys. Lett. **73**, 262 (1998).
[5] Calculations were performed using G. L. Snider's 1D Poisson solver.
[6] G. L. Snider, I.-H. Tan, and E. L. Hu, J. Appl. Phys. **68**, 2849 (1990).
[7] I.-H. Tan, G. L. Snider, L. D. Chang, and E. L. Hu, J. Appl. Phys. **68**, 4071 (1990).
[8] L. Pfeiffer, E. F. Schubert, K. W. West, and C. W. Magee, Appl. Phys. Lett. **58**, 2258 (1991).
[9] Schrodinger equation for this potential can be solved analytically, see L. D. Landau and E. M. Lifshitz, *Quantum Mechanics: Non-Relativistic Theory* (Pergamon Press, Oxford, 1991).
[10] T. Heinzel *et al*., Phys. Rev. **B61**, R13353 (2000).
[11] I. A. Larkin and V. B. Shikin, Phys. Lett. **A151**, 335 (1990).